Sound wave propagation and existence of a two step relaxation process in a glass-former melt

M. Soltwisch,[1] G. Ruocco,[2] B. Balschun,[1] J. Bosse,[1] V. Mazzacurati,[2] and D. Quitmann[1]
[1]*Fachbereich Physik, Freie Universität, Berlin, D-14195 Berlin, Germany*
[2]*Universitá di L'Aquila and Istituto Nazionale di Fisica della Materia, I-67100, L'Aquila, Italy*
(Received 15 January 1997)

The velocity and damping of longitudinal and transverse sound waves of a prototypical glass-forming melt, *m*-tricresylphosphate, are studied over a very wide frequency span by an ultrasonic and a light scattering experiment (10^7 and 10^{11} rad/s). In the Brillouin light scattering measurements, the central quasielastic line has been also analyzed. Unpublished data on velocity and damping (frequency $\approx 10^9$ rad/s) are also included in the present analysis. A quantitative analysis of the data gives good agreement for individual spectra as well as for the general temperature trends. The analysis is based on the existence of fast (β) and slow (α) relaxation processes in the liquid. A phenomenological description of a two step relaxation function is proposed, and the phenomenological parameters [relaxation times, τ_α and τ_β, relative weight, $\tilde{f}(T)$, etc.] of the two relaxation processes are derived. As a consequence of the two step relaxation process, we propose to revise the concept of ''infinite frequency'' (c_∞) sound velocity, introducing two characteristic sound velocities, one which applies if $\omega\tau_\beta \gg 1$, c_∞, and one, $c_{\infty\alpha}$, which describes the elastic response of the liquid at frequency higher than $1/\tau_\alpha$ but smaller than $1/\tau_\beta$. Within the framework of a two step relaxation process, the meaning of ''nonergodicity'' parameter of mode-coupling theory and its relation with $\tilde{f}(T)$ are also discussed. The weight $\tilde{f}(T)$ is found to decrease monotonically from near 1 to near 0.4 between T_g and $1.5T_g$. The comparison of our findings with the predictions of the mode-coupling theory shows qualitative accord in several important points. [S1063-651X(97)07212-7]

PACS number(s): 64.70.Pf

I. INTRODUCTION

The existence of two very different relaxation processes, a slow (α) and a fast (β) one, in glass-forming melts, and the mechanism of their interplay in the liquid-glass transformation, are to our present knowledge at the basis of the understanding of how and why a glass forms from equilibrium melt.

The slow relaxation time $\tau_\alpha(T)$ is ''the characteristic'' relaxation time which increases dramatically as the glass transition temperature T_g is approached from the liquid side. On the contrary, the fast relaxation time τ_β is believed to be weakly T dependent, and possibly the same in the melt and in the glass; see, e.g., Fig. 11.9 in Ref. [1]. Beyond the values of both time constants, their relative strength or weight is decisive for the dynamics of the system. Following the analysis of mode-coupling theory (MCT) [2], valid for the case $\tau_\alpha \gg \tau_\beta$, we introduce the weight of the τ_α relaxation step as the ''plateau height'' $\tilde{f}$ of the relaxation function k_L [see below, Eq. (6)].

The τ_α time has been studied extensively, since the condition on the characteristic frequency ω of an experiment for optimum sensitivity, $\omega\tau_\alpha \approx 1$, can be met by many experiments, including ultrasonics ($\omega \approx 10^7$–10^8 rad/s) and Brillouin light scattering ($\omega \approx 10^{11}$ rad/s). The fast time constant τ_β, however, is much more difficult to observe in experiment unambiguously, being situated in the 10^{-12}-s range. Its influence on sound waves, however, could be shown in Brillouin scattering experiments [3,4].

In this paper we present a sound wave study on metatricresylphosphate (*m*TCP), a fragile molecular glass former, becoming a glass at $T_g = -68$ °C. We measured the sound velocity and its damping over a broad range of temperatures from the true liquid into the glass state, and measured these values using a broad range of frequencies.

The propagation of a longitudinal acoustic (LA) wave produces local density variations with a mean frequency $2\pi\nu_L = \omega_L = c_L q$, c_L being the apparent LA velocity of sound and q the magnitude of the wave vector.

With Brillouin light scattering (BS), one selects a certain q value, i.e., $q = (4\pi n/\lambda)\sin(\theta/2)$ (where n is the index of refraction, λ the laser wavelength, and θ the scattering angle) and measures the position ω_L and the width Γ_L of the phonon line. The same can be done for transverse acoustic (TA) waves, determining ω_T and Γ_T. Using visible laser light for BS and $\theta = 90°$, the observed frequencies ν_L and ν_T are in the range of a few GHz (see Fig. 1). Applying ''impulsive stimulated thermal scattering'' (ISTS) [5], Deeg and Diercksen [6] could strongly reduce the q values, and measured the dynamics of *m*TCP at frequencies of $\nu_L \sim 50$–100 MHz. A third experiment that we performed on the same substance was an ultrasonic measurement (US). This brought down the frequency range to about $\nu_L \sim 2$ MHz.

In summary, here we measure velocity and damping of LA sound waves as a function of temperature over a frequency span of nearly four orders of magnitude (TA, only BS). This allows us to determine the shape of the underlying relaxation functions, which were found to be by no means simple stretched exponentials. Rather, they consist of a narrow ($1/\tau_\alpha$, strongly T dependent) line and a broad ($1/\tau_\beta$, nearly T-independent) line. We also compare our results with the prediction of the MCT [2,7–9], the only formalized theory of the glass transition which describes the behavior of the density-density correlation function when T approaches

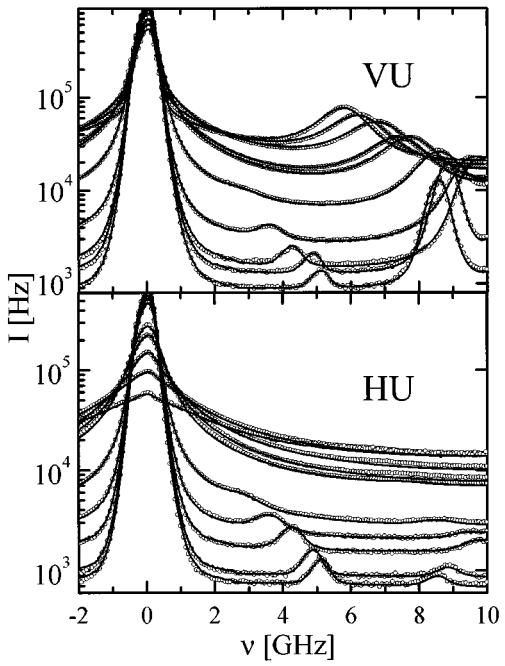

FIG. 1. Fabry-Perot spectra of *m*TCP in the VU (upper panel) and HU (lower panel) scattering configurations. The temperatures for each set are, from bottom to top, -65, -55, -35, -15, $+5$, 22, 35, 53, 74 and 94 °C. The curves through the points are the global fit curves (including resolution broadening). In the lowest two spectra the LA lines seen belong to the next FP order.

T_g. It is worth noting that the LA sound waves *are* density fluctuations (though they are determined by bulk as well as shear modulus; see Sec. V C below), and, therefore, a direct comparison with the MCT predictions can be easily made. On the contrary, up to now, most comparisons of MCT with experiments have considered depolarized light scattering spectra. There it is very often not clear whether these spectra relate to the orientational relaxation of individual molecules, or to the four particle correlation function of the induced effects as, for example, the dipole-induced-dipole (DID) mechanism [10].

We have studied the *m*TCP polarized and depolarized spectra, in a frequency range covering from the central line out to the boson peak region. The temperature range was -70–220 °C. The central line width is compared with results from NMR [11], which measures the orientational relaxation of the molecule.

Considerable effort is made here to arrive at quantitative descriptions (fits) of the measured spectra, of the sound velocities and the line widths vs T. The aim is to allow a comparison with some of the predictions of MCT, in particular the existence and the weight of the fast relaxation time. However, deviating from MCT, we have chosen an analytical approximate expression for the relaxation functions k [see Eqs. (4)–(6)], so that a straightforward interpretation of the parameters is possible.

The paper is organized in the following way: In Sec. II we briefly describe the experimental conditions. Section III presents the viscoelastic formulation for the LA and TA Brillouin lines and for the central line. Section IV gives the results from the different fits. In Sec. V we discuss the results and compare them with the MCT scenario.

II. EXPERIMENT

The *m*TCP samples for light scattering were prepared as described in Ref. [12] by heating under vacuum (for purification), and pressing through a micropore filter into a quartz cell of $2\times10\times30$-mm^3 inner dimension, which was flame sealed. The same sample was measured on two spectrometers, the laser beam entering at the narrow side (2 mm).

The first series of light scattering spectra were taken using a piezoelectrically scanned triple pass Fabry-Pérot (Burleigh, FU Berlin), while the second used a high resolution grating spectrograph (SOPRA, L'Aquila [13]). The two setups were conventional: argon ion laser ($\lambda = 514$ nm operating in single mode thanks to an intracavity etalon; 200 mW); 90° scattering geometry; the sample cell was in a furnace or cryostat with ± 1-K temperature accuracy and stability.

In Fig. 1, Fabry-Perot (FP) spectra of *m*TCP are presented [upper part VU polarization, lower part HU (the pairs of capital letters describe incoming and scattered beam polarization conditions with V vertical, H horizontal, U no polarization discrimination, relative to the scattering plane); note the logarithmic ordinate scale]. The TA line was measured with good statistical significance, although it is about a factor 10^2 weaker than the LA line. Beyond the data reported here, the region of the boson peak was included in the study [14]. Preliminary results concerning the transverse modes have been published before [15].

An independent experiment (US) allowed the study of sound waves at low frequency. Basically it consists of a Mach-Zehnder interferometer where one light beam traverses the sample cell at a given distance from the surface at which a sound pulse (LA) is generated by an infrared laser pulse (for further details, see Ref. [16]). The experimental conditions (IR absorption depth, IR laser pulse duration, sound velocity) set the center of the effective frequency band in the present case to $\nu \simeq 2$ MHz. The experimental results, viz. the observed sound velocity $c_L(T)$ and the damping $\Gamma_L(T)$, both valid for this frequency, are included in Figs. 2 and 3.

Additionally in the present analysis we use unpublished results of ISTS measurements on *m*TCP by Deeg and Diercksen [6]. The ISTS experiment consists of two picosecond laser pulses that produce a thermal grating which in turn induces two sound waves in exactly opposite directions ($\mathbf{q}$, $-\mathbf{q}$). A second probe laser observes under Bragg condition the time evolution of the standing wave pattern, which oscillates at $2\nu_L$. This setup allows a determination of the damping directly on the time axis. Effective wavelengths used were 18 and 34 μm, respectively, which correspond to Brillouin frequency $\nu_L \approx 50$–100 MHz. This is two orders of magnitude below the frequency of the 90° light scattering experiments while the ultrasonic experiment works again two orders of magnitude lower in frequency than the ISTS. The results of all three experiments are summarized in Figs. 2 and 3 and are discussed in Secs. IV and V.

III. MODEL

Each light scattering spectrum (Fig. 1) in the frequency region discussed here is considered as a sum of a quasielastic central line (C), and transverse and longitudinal phonon lines (T and L). A relatively small base caused mainly by the

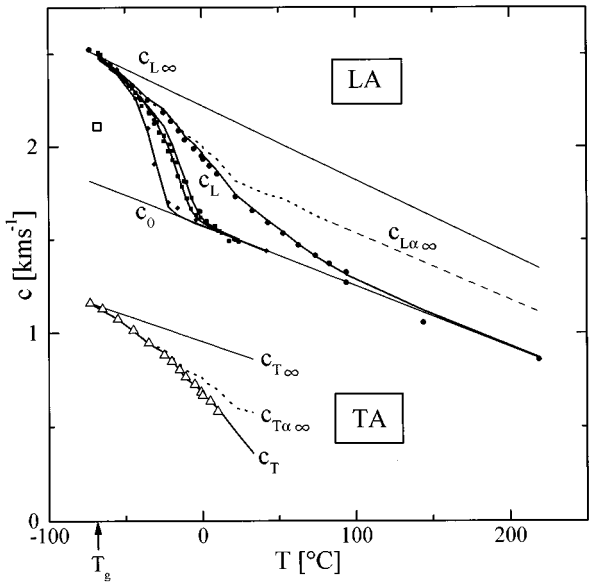

FIG. 2. Sound velocities in *m*TCP. Upper part: LA velocities. Full points are the ''experimental'' velocities as defined in Sec. IV A. The full straight lines are $c_o(T)$ and $c_{L\infty}(T)$, the broken line is $c_{L\alpha\infty}$ from Eq. (7). The bent full curves are the model results for the apparent sound velocity $c_L(T)$: the leftmost curve is from ultrasonics (2 MHz), the two middle curves are for ISTS (50 and 100 MHz, respectively), and the rightmost curve is for the Brillouin measurements (10 GHz). The single open square is $c_{B\infty}$ at $T=-65\,°\mathrm{C}$; see the discussion in Sec. V C. Lower part: TA velocities from Brillouin measurements. The upper curve is $c_{T\infty}(T)$, the broken line is $c_{T\alpha\infty}$, and the lower curve is $c_T(T)$. The open triangles are from local fits (DHO).

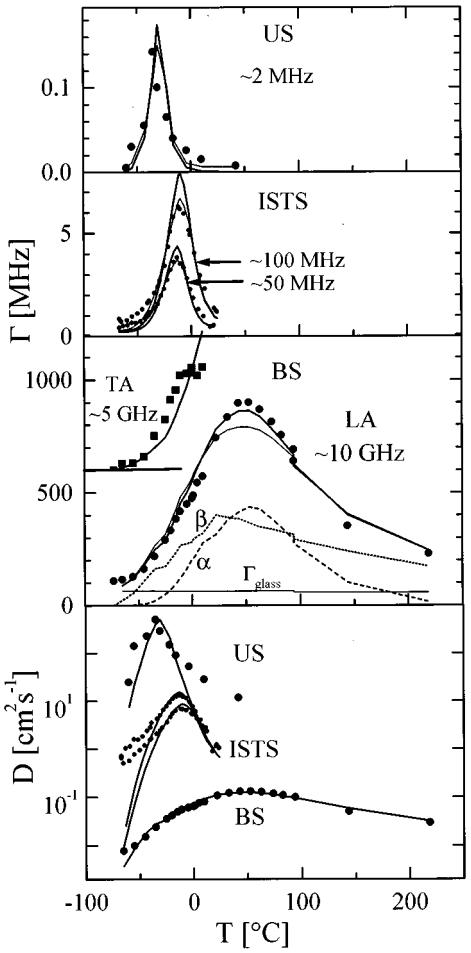

FIG. 3. Line widths Γ_L and Γ_T for *m*TCP. Numbers for widths Γ and frequencies are in MHz (not rad/s). Upper three sets: plotted on a linear scale (note the very different frequency ranges). Full circles are the ''experimental'' Γ_L, full squares are ''experimental'' Γ_T (note the *y* shift of 600 MHz to avoid overlap). Full curves are from the model fit; see text. The break for the Brillouin values at 90 °C occurs because the three highest *T* values have been measured at a slightly lower *q* with SOPRA. Also inserted in the Brillouin part are the three contributions $\Gamma_L(\alpha)+\Gamma_L(\beta)+\Gamma_{\mathrm{glass}}=\Gamma_L$, which build up the full width of the LA phonons (see Sec. IV B). Lowest set: Γ_L plotted as $D=2\Gamma_L/q^2$ on a logarithmic scale.

low-frequency wing of the boson peak is of no relevance here:

$$I(q,\omega)=I_C(q,\omega)+I_T(q,\omega)+I_L(q,\omega). \tag{1}$$

All these scattering events (C,L,T) are affected in different ways by the relaxation processes.

A. Longitudinal acoustic line (L)

For phonons having wavelengths large compared to atomic distances (as in the present cases), the viscoelastic description is well established (see, e.g. , Ref. [17]), and its parameters are not q dependent. For LA waves, one usually considers the adiabatic sound velocity $c_o(T)$ and the high-frequency value $c_{L\infty}(T)$ as the primary parameters. The LA Brillouin spectrum is expressed in terms of a relaxation kernel as follows :

$$I_L(q,\omega)=I_L\phi_N''(q,\omega)=\frac{I_L}{\pi}\mathrm{Im}\left\{\frac{c_o^2q^2\omega^{-1}}{c_o^2q^2-\omega^2-\omega K_L(q,\omega)}\right\}, \tag{2}$$

where the subscript index N indicates the number density, and I_L takes into account all the constant factors not relevant here. For the relaxation kernel $K_L(q,\omega)$ we made the following ansatz:

$$K_L(q,\omega)=(c_{L\infty}^2-c_o^2)q^2k_L(\omega). \tag{3}$$

As explained above, the frequency spectrum $k_L(\omega)$ of the relaxation kernel is written as the sum of two terms. The first, describing the slow α relaxation, has a linewidth $\Gamma_{L\alpha}=1/\tau_{L\alpha}$ which vanishes when $T\to T_g$, and changes strongly above T_g. It can be represented by

$$k_{L\alpha}(\omega)=\frac{1}{\omega}\left(\frac{1}{[1+\omega/(i\Gamma_{L\alpha})]^{\beta_{CD}}}-1\right). \tag{4}$$

The second, the fast β relaxation, has a linewidth $\Gamma_{L\beta}=1/\tau_{L\beta}$, and it is written as

$$k_{L\beta}(\omega)=\frac{1}{\omega}\left(\frac{1}{1+[\omega/(i\Gamma_{L\beta})]^{\beta_{CC}}}-1\right). \tag{5}$$

They combine to the total relaxation spectrum with weights $\tilde{f}_L(T)$ and $1-\tilde{f}_L(T)$, respectively:

$$k_L(\omega)=\tilde{f}_L k_{L\alpha}(\omega)+(1-\tilde{f}_L)k_{L\beta}(\omega). \tag{6}$$

Here $\beta_{CD}\leqslant 1$ is the Cole-Davidson stretching parameter, while $\beta_{\mathrm{CC}}\leqslant 1$ is the Cole-Cole parameter. We used $\beta_{\mathrm{CC}}=1$, because the widths and positions of the phonon lines in our measurements were not sensitive to a possible stretching in the β process. The $\tilde{f}_L$ value, $0<\tilde{f}_L(T)<1$, defines the relative weight of the two processes. $\Gamma_{L\beta}$ is expected to vary very weakly with T, and an Arrhenius ansatz was used in the data analysis, i.e., $\Gamma_{L\beta}=\Gamma^0_{L\beta}\exp(-T_\beta/T)$, with $T_\beta\approx 30$ K $\ll T_g$.

A similar ansatz for $I_L(q,\omega)$, using two relaxation processes, has been already introduced [3] mainly to explain the LA linewidth observed in an inorganic glass former.

The effect of a two step relaxation, Eq. (6), will be a two step change of sound velocity. It is suggested here, therefore, that the primary elastic parameters are the high-frequency sound velocity $c_{L\infty}$ (measurable if $\omega\tau_{L\alpha}\gg 1$ *and* $\omega\tau_{L\beta}\gg 1$) and the low-frequency sound velocity $c_o(T)$ (measurable if $\omega\tau_{L\alpha}\ll 1$ *and* $\omega\tau_{L\beta}\ll 1$). An additional characteristic velocity $c_{L\alpha\infty}$ (measurable if $\omega\tau_{L\alpha}\gg 1$ *but* $\omega\tau_{L\beta}\ll 1$) may be defined in the present two step relaxation model. The latter corresponds to $c_\infty(T)$ of experiments (e.g. ultrasonics) in which the frequencies are much smaller than $1/\tau_{L\beta}$. The scenario proposed here furnishes a straightforward explanation of the fast drop of $c_\infty(T)$, i.e., $c_{L\alpha\infty}(T)$ in our terms, right above T_g, as will become clear later (Sec. V B).

The usual modulus which is relaxed by the α process, $c^2_{L\alpha\infty}-c^2_o$, is thus replaced by

$$c^2_{L\alpha\infty}-c^2_o \Rightarrow \tilde{f}_L(c^2_{L\infty}-c^2_o). \tag{7}$$

The parameter $\tilde{f}_L(T)$ can thus be derived from the position of the LA line, once $c_{L\infty}(T)$ is known. In the following we will assume that $c_{L\infty}$ has only a weak temperature dependence, and we will define it to be linear with T, and vanishing at the same temperature as $c_o(T)$:

$$c_{L\infty}(T)=c_{L\infty}(T_g)-(T-T_g)\frac{c_{L\infty}(T_g)}{c_o(T_g)}c'_o. \tag{8}$$

The slope $c'_o=dc_o(T)/dT$ is taken from the high-temperature part of the US measurements: $c'_o=3.26m/(sK)$. Slightly different choices of the slope of $c_{L\infty}(T)$ do not seriously affect the results for $\tilde{f}_L(T)$ and $\Gamma_{L\beta}(T)$.

The spectrum equation (2) consists of the two Brillouin peaks and a central line which extends out just to the Brillouin peaks, but not further. This central line is the well known Mountain peak which has the shape of the relaxation kernel, Eq. (6). This shape is not q dependent, contrary to the Brillouin positions and widths. The width of the Brillouin lines is directly $\mathrm{Im}\{K_L(q,\omega_L)\}$ where ω_L is the peak frequency. Let us start from the simplified case where ω_L is much larger than $\Gamma_{L\alpha}$ and $\Gamma_{L\beta}$ [as always assumed in MCT, a theory which gives a rigorous formulation of the Mountain peak, while we model it with the simplified ansatz of Eq. (6)]. Then one can directly derive the ratio of the intensity under the central peak of $I_L(q,\omega)$ to its total intensity. The result is determined only by the moduli, and gives

$$f_{\mathrm{Total}}=1-\frac{c^2_0}{c^2_{L\infty}}. \tag{9}$$

The nonergodicity parameter f_{MCT} (according to MCT) takes into account only the α contribution to the central peak in Eq. (2). According to Eq. (7) it results that

$$f_{\mathrm{MCT}}=1-\frac{c^2_0}{c^2_{L\alpha\infty}}=\frac{\tilde{f}_L}{\tilde{f}_L+\dfrac{c^2_0}{c^2_{L\infty}-c^2_0}}. \tag{10}$$

B. Transverse acoustic line (T)

It is clear that the analog of c_o of LA waves for TA waves is zero (low-frequency shear waves are overdamped in the liquid). For clarity, we still distinguish between the $\tilde{f}$ parameters $\tilde{f}_L(T)$ and $\tilde{f}_T(T)$. Then

$$I_T(q,\omega)=\frac{I_T}{\pi}\mathrm{Im}\left\{\frac{-1}{\omega+K_T(q,\omega)}\right\}, \tag{11}$$

with

$$K_T(q,\omega)=c^2_{T\infty}q^2[\,\tilde{f}_T k_{T\alpha}(\omega)+(1-\tilde{f}_T)k_{T\beta}(\omega)\,]. \tag{12}$$

We use the same structure for the frequency dependence of the relaxation kernel as was given for the LA modes in Eqs. (4) and (5).

C. Central line (C)

Although the present work focuses on the sound waves, the central line (CL) has to be included in the analysis, being essential for the Brillouin region because of its high-frequency tail. In contrast to the LA and TA lines, which in a 90°-scattering experiment appear only in VV and VH geometry, respectively, the central line is fully depolarized. No matter what is the specific scattering mechanism—here presumably light scattering from molecular reorientational dynamic—we assume that it has directly a relaxational shape with no q dependence.

$$I_C(\omega)=\frac{I_C}{\pi}\mathrm{Im}\{\tilde{f}_C k_{C,\alpha}(\omega)+(1-\tilde{f}_C)k_{C,\beta}(\omega)\}. \tag{13}$$

Again we use the same formulation [Eqs. (4) and (5)] for its frequency dependence. For the VU spectra we had to add an additional delta function $\delta(\omega)$, which accounted for the polarized straylight.

IV. RESULTS

A. Fits

The parameters of the model were mainly derived from least-squares fits of the quoted expressions to the measured Brillouin spectra, as the examples in Fig. 1 show. The fit routine was usually applied simultaneously to sets of spectra

(up to 25), or to individual spectra. It takes into account the apparatus broadening by numerical convolution with the experimentally determined resolution functions. In the case of FP spectra the presence of neighboring orders (up to ten orders) is taken into account. Some of the fitting parameters are common to the whole set of spectra [e.g., $c_{L\infty}(T_g)$], while others may be individually different (e.g., I_L).

To compare ''experimental'' line positions and linewidths ($\omega_L = c_L q$ and Γ_L) with those which follow from the model, for FP and SOPRA spectra we have fitted simple damped oscillator line shapes to each spectrum individually. The results appear as ''experimental'' points in Figs. 2 and 3. The ''theoretical'' positions and widths are read numerically from the theoretical spectra prior to convolution with the apparatus function. They appear as thick smooth lines. For easier comparison with the moduli, we generally plot c_L instead of ω_L.

The ''experimental'' points for US (c_L, τ_L) and ISTS (ω_L, τ_L) were derived from the spectra by individual fits on time axis and converted to (ω_L, Γ_L) pairs. To compare them with the model used here, we again derived the ''theoretical'' positions and widths ω_L and Γ_L due to Eq. (2). The minimization process of the squared differences (χ^2) was performed by then changing the model parameters.

Performing preliminary fits to LA and TA sets of spectra for the case of Brillouin scattering, we found that at all temperatures $\Gamma_{L\alpha}(T) \approx \Gamma_{T\alpha}(T)$ and $\Gamma_{L\beta}(T) \approx \Gamma_{T\beta}(T)$. Also, $\tilde{f}_L(T)$ and $\tilde{f}_T(T)$ follow each other closely, the difference $|\tilde{f}_L(T) - \tilde{f}_T(T)| < 0.1$ at all temperatures. Thus we use simply $\Gamma_\alpha(T), \Gamma_\beta(T)$ and $\tilde{f}(T)$ in Eqs. (6) and (12).

For the Cole-Davidson stretching parameter of the α process $\beta_{\eta \mathrm{CD}}$ ($\eta = L, T, C$) for all three different types of spectra we found the common value $\beta_{\eta \mathrm{CD}} = 0.4 \pm 0.1$, with $\beta_{C,\mathrm{CD}}$ having the strongest statistical significance. To determine $\beta_{C,\mathrm{CD}}$, we additionally used a set of wide energy range HV spectra measured by a SOPRA double monochromator [14,18].

For the widths of the central line $\Gamma_{C\alpha}$ we find good agreement with values derived from a NMR experiment [11], which measured the reorientational relaxation time of the molecule. So we write $\Gamma_{C\alpha} \approx \Gamma_{\mathrm{NMR}} \approx \Gamma_{\mathrm{rot}}$ (see Fig. 4, lowest curve and squares). The additional broadening due to translational motion is for these small q values negligible.

The NMR Cole-Davidson parameter was found [11] to be $\beta_{\mathrm{NMR,CD}} = 0.38$, which is confirmed by our light scattering results. The value $\tilde{f}_C$ was found to be ≈ 1, i.e., we could fit the wide range HV spectra (SOPRA) with the stretched Cole-Davidson function up to the boson peak region; the boson peak intensity amounted to only about 10% of the central line intensity [18].

According to these findings, we make the global ansatz that (i) the same memory function $k(\omega)$ determines both LA and TA complex moduli with $\beta_{CD} = 0.4$; and (ii) the values of $\Gamma_{C\alpha}(T)$ and $\Gamma_{L\alpha}(T) = \Gamma_{T\alpha}(T) = \Gamma_\alpha(T)$ have the same temperature dependence, but may be different by a common factor $\hat{k} = \Gamma_\alpha(T)/\Gamma_{C\alpha}(T)$.

A second series of fits is performed to the whole sets of spectra (FP spectra for VU and HU; SOPRA spectra for VV and HV; US and ISTS for LA parameter sets only; global parameters: $c_0(T)$, $c_{L\infty}(T)$, $c_{T\infty}(T)$, $\hat{k}$; local parameters: $\tilde{f}(T)$, total intensities and backgrounds for the FP and SOPRA spectra). The resulting fit curves for the FP spectra are included in Fig. 1, and are seen to be very satisfactory.

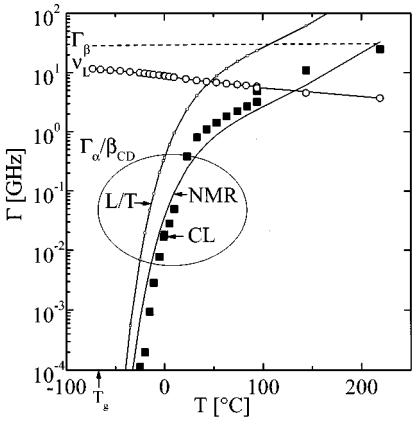

FIG. 4. Effective width parameters $\Gamma'_\alpha = \Gamma_\alpha / \beta_{\mathrm{CD}}$ ($\beta_{\mathrm{CD}} = 0.4$) and Γ_β of the relaxation functions in GHz (not rad/s). Γ_β is upper dashed line. Γ'_α are the bent curves. The lower bent curve is Γ'_{NMR} while the upper one is $\Gamma'_\alpha(T) = 10\Gamma'_{\mathrm{NMR}}(T)$. The experimental central linewidths (full squares) follow closely Γ'_{NMR}, while the offset of one order of magnitude to the Γ'_α curve derived from the LA and TA Brillouin fits is remarkable. Note the merging of this Γ'_α curve and the Γ_β curves at about 100 °C. Around this temperature one may enter the single relaxation region. The lower nearly straight curve is the Brillouin energy $\nu_L = c_L q / 2\pi$ (open circles are the experimental values). The crossing point of this curve with the Γ_α curve corresponds to the maximum damping of the ~ 10-GHz sound waves; see Fig. 3.

B. Parameters

The apparent sound velocities obtained are presented in Fig. 2, for LA and TA waves from Brillouin spectra, and for LA from US and ISTS. The full lines are the results of the global fits, using the model described above. They follow very well the three experiments: US (left most data); ISTS (the two middle sets) from Deeg and Diercksen; and BS (right hand data). The dashed line in the LA part is a plot of $c_{L\alpha\infty}(T)$ obtained from Eq. (7). The dashed line in the TA part is correspondingly $c_{T\alpha\infty} = \sqrt{\tilde{f}(T)}\, c_{T\infty}$.

Figure 3 presents, in the upper three parts, the width parameters Γ_L and Γ_T (from BS) and Γ_L (from US and ISTS). In the lower part they are plotted as kinematic viscosities $D = 2\Gamma_L / q^2$, on a logarithmic scale.

The smooth thick curves in Fig. 3 are the theoretical dependencies for $\Gamma_{L,T}$ as obtained from the model. Again the curves follow the experimental points well for the four frequencies. The fact that both the bending down of sound velocities in Fig. 2 and the width maxima in Fig. 3 are well and even quantitatively described, supports the model chosen and the parameters found. Discrepancies are seen, especially in the 2–100-MHz data for Γ, on the level of about 10% of the maximum of each curve, and in a residual width in the glass state for LA widths. We account for the latter by inserting a

constant additional Γ_{glass}, displayed for the Brillouin widths as the lowest straight line.

However, in the fitting process, especially of the lower frequency data (US and ISTS) it turned out that the time constant $\tau_{L\alpha}=1/\Gamma_{L\alpha}$ entering Eqs. (2) and (11), via Eq. (4), had definitely to be chosen shorter than for the CL, Eq. (13). Fits were best for $\Gamma_{(T,L)\alpha}\approx 10\Gamma_{C\alpha}$, with an estimated uncertainty of about 30% for the factor $\hat{k}=10$. One can improve the fit quality especially for ISTS by choosing $\hat{k}=7$ instead of 10, and a Cole-Davidson (CD) parameter $\beta_{\text{CD}}=0.3$ instead of 0.4, respectively. These are the thinner full lines in the linear displays of Γ_L.

For the Brillouin widths in Fig. 3, we plot two further theoretical curves (indicated as α and β). The α curve was computed by setting Γ_β to a very high frequency, so that only the α process produces a linewidth $\Gamma_L(\alpha)$ (Γ_{glass} was set to zero). The β curve is then simply $\Gamma_L(\beta)=\Gamma_L-\Gamma_L(\alpha)$. Its increase with T above T_g reflects the onset of the fast relaxation. The jitter of this curve is mainly due to the locally determined $\tilde{f}$ factors.

Figure 4 presents the various effective widths $\Gamma_\alpha/\beta_{\text{CD}}$ (bent curves and squares) and Γ_β (dashed line). We note that $\Gamma_{C\alpha}\approx\Gamma_{\text{NMR}}$ in a good approximation, and that the temperature dependence of the α-relaxation process agrees well between NMR or CL on the one hand, and LA and TA on the other (though their values differ, as was just mentioned). The open circles are the frequencies of the phonons from BS. The crossing of $\Gamma_{L\alpha}/\beta_{\text{CD}}$ with the frequency curve occurs around the same temperature where one observes the width maximum ($\omega\tau_\alpha\beta_{\text{CD}}\sim 1$) of the α curve in Fig. 3. But this width is only half of the measured width. Thus one needs the fast process, curve β in Fig. 3.

This fast process $k_\beta(\omega)$ is found to have an effective relaxation time in the range

$$\tau_\beta=0.5\times 10^{-11}\ \text{s}, \quad \Gamma_\beta=2\pi\times 30\ \text{GHz},$$

which is weakly temperature dependent ($T_\beta\approx 30$ K).

Figure 5 presents the fit results for $\tilde{f}(T)$, $f_{\text{MCT}}(T)$, and $f_{\text{Total}}(T)$. The locally fitted $\tilde{f}(T)$ value decreases monotonically approaching 0.45 effectively around 35 °C, i.e., at $T^*\approx 1.5T_g$. Above a temperature $T\approx 1.6T_g$ the $\tilde{f}$ value was kept constant, which reflects the fact that Γ_α and Γ_β are of the same size, so that different $\tilde{f}$ values produce the same relaxation in any case. In other words, there is only a single relaxational process above that T (see the merging of α and β maxima in the upper part of Fig. 6 and Γ_α and Γ_β at higher T in Fig. 4). In contrast to the sound wave lines, the central line requires $\tilde{f}_C=1$ in the full temperature range studied.

At low temperatures where $\omega_L\tau_\alpha\gg 1$, nearly one half of the LA spectral intensity appears as a central part (Mountain line), which broadens and merges with the phonon line as τ_α shortens at higher T; see g_{Mount} and g_{phon} in Fig. 5. This spectral component was not decisive in the fits to the Brillouin spectra, because it was always masked by the much stronger central line. Only the propagating sound waves (Brillouin lines) were decisive.

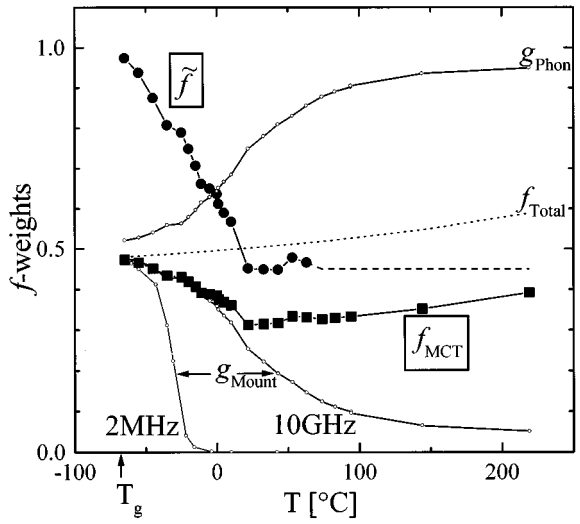

FIG. 5. f factors, as derived from LA and TA lines. Connected full circles : $\tilde{f}(T)$, the slowly relaxing part of $k(\omega)$. The dashed part of the curve denotes the region where Γ_α and Γ_β are of the same magnitude, so that the $\tilde{f}$ value loses its mathematical meaning. It was fixed for the fitting procedure at $\tilde{f}=0.45$. Connected full squares : f_{MCT} from Eq. (10). Short dashed line: f_{Total} from Eq. (9). Lower curves: g_{Mount}, integral of central part of $\phi''(q,\omega)$ for BS ($\sim$10 GHz) and for US ($\sim$2 MHz), respectively. The upper curve is $g_{\text{phon}}=1-g_{\text{Mount}}$, the relative phonon intensity for BS.

C. Fluctuation spectra

Finally, Fig. 6 summarizes the susceptibility spectra $\chi''(q,\omega)=\omega\phi_N''(q,\omega)$ at different temperatures, using the parameters obtained in the fits for a set of temperatures and different momentum transfers q in a log-log display. The upper panel of Fig. 6 shows two contributions of the fluctuation spectra ϕ_N'' (which are the two contributions to the Mountain peak): One, with a short time constant τ_β, with a maximum at about 30 GHz (nearly T independent), increases in weight with increasing T. The other contribution has a longer and strongly T-dependent time constant $\tau_\alpha(T)$, and decreases in weight with T. These spectra were simulated, choosing a phonon frequency of 20 THz which is outside the displayed region.

The lower part repeats the full Mountain part for two temperatures ($T=-35$ and $+94$ °C) but it also shows the normalized LA phonon spectra $\phi_N''(q,\omega)$ for the three experiments (US, ISTS, and BS, from left to right) for these two temperatures. One observes that the existence of a phonon ''cuts off'' the central line for frequencies larger than the phonon frequency. It is a consequence thereof that the full β-relaxational part can possibly be observed only for $1/q$ values in the Angstrom region which is the range of x-ray wavelengths or atomic distances (the rightmost pair is a simulation using $q=0.2$ Å^{-1}).

V. DISCUSSION

A. Slow and fast time constants

First we turn to the relaxation processes as described by $k(\omega)$. From many experiments, old and recent, it has become

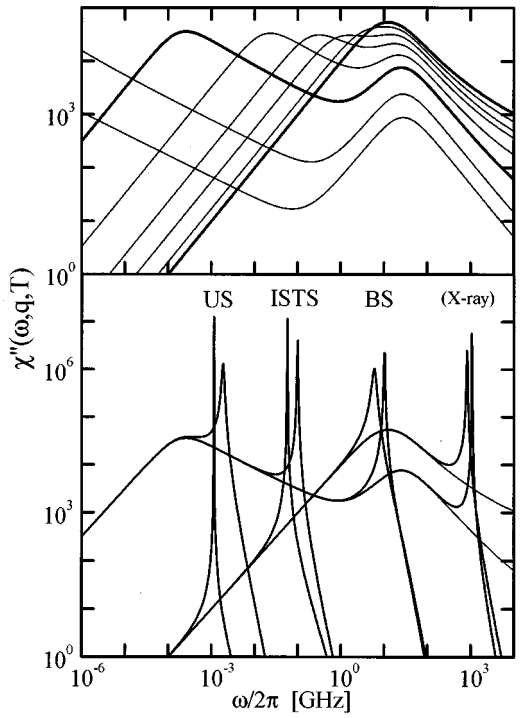

FIG. 6. Susceptibility plot of $\phi''(q,\omega)$ for selected q and T values. Plotted is $\chi''(q,\omega)=\omega\phi_N''(q,\omega)$ vs ω on a double logarithmic scale [see Eqs. (2) and (3)]. For the parameters chosen, see Sec. IV B, Figs. 2, 4 and 5, and Table I. The β peak is located around 30 GHz, and its relative intensity increases with $1-\tilde{f}(T)$ compared to the α peak. The α peak moves with increasing T from left to right, and loses weight. Upper panel: T dependence ($T=-65\ldots+94\,^{\circ}\mathrm{C}$ as in Fig. 1). In order to display the full relaxation spectrum in this graph, the phonon frequency was shifted out of the picture (20 THz). Lower panel: q dependence, and phonon lines included. From left to right the three double sets are each for -35 and $+94\,^{\circ}\mathrm{C}$, and for the following q values: $q\approx 4\ \mathrm{mm}^{-1}$ ($\nu_L\approx 2$ MHz, US), $q\approx 0.3\ \mu\mathrm{m}^{-1}$ ($\nu_L\approx 100$ MHz, ISTS), and $q\approx 30\ \mu\mathrm{m}^{-1}$ ($\nu_L\approx 10$ GHz, 90°BS). They indicate the experimental range of frequencies used in this analysis. The most right set of Brillouin peaks is a simulation with $q\approx 2\ \mathrm{nm}^{-1}$ ($\nu_{\mathrm{ph}}\approx 1$ THz, accessible only with inelastic x-ray scattering).

clear that at least two relaxations and stretching have to be included in writing down the frequency dependent elastic moduli for both LA and TA waves. The claim is tested here on *m*TCP, and there are three other LA Brillouin studies which showed the need for two relaxation times, viz. [3] ($GeSBr_2$), [4] ($CaKNO_3$), and [19] (As_2O_3).

The temperature dependence of $\Gamma_{\eta\alpha}(T)$ ($\eta=L,T,C$) follows the NMR result [11] closely, as was to be expected. However it came out very clearly, especially from the lower-frequency measurements (US, ISTS), that Γ_{NMR} had to be multiplied by $\hat{k}=10(\pm 3)$ in order to describe well the velocity cross over and the peak of the damping ($\Gamma_{(L/T)\alpha}\simeq 10\Gamma_{\mathrm{NMR}}$). There is very little effect of the fast β process at these lower frequencies, so that one observes in US and ISTS essentially the rapid narrowing of Γ_α. On the other hand, fitting the CL we find for its widths $\Gamma_{C\alpha}\simeq\Gamma_{\mathrm{NMR}}$, i.e., good agreement with NMR. For the CD stretching parameter the value $\beta_{\mathrm{CD}}=0.4\pm 0.1$ describes well all the relaxational kernels $k_{\eta\alpha}$ *and* agrees with NMR. So we are forced to state a serious discrepancy for the α -correlation time prefactor $\hat{k}$, if one compares collective damping (macroscopic; long wavelength sound waves) with individual motion (microscopic; reorienting molecules).

At present we can only speculate on possible reasons(s) for this apparent discrepancy. First we note that a similar effect was recognized in Refs. [20–22]. At least two points should be taken into consideration. (i) Damping of elastic waves proceeds through relaxation of center of mass motion, as well as through relaxation of reorientation. (ii) If the decisive unit for viscous flow is not the single molecule, but is of intermediate size, then the first relaxation of a single molecule within may allow relaxation of the unit. Assume now that this process concerns N molecules, of which each relaxes (reorients) on the average after time $\tau_{\alpha,\mathrm{rot}}$; then the first relaxation process will occur after $\tau_{\alpha,\mathrm{rot}}/N$.

In the first of the previous studies already mentioned, we analyzed the BS of $GeSBr_2$ [3] (four different scattering angles, LA sound). The single relaxation fit also failed, especially at higher q and higher temperatures. This failure could be removed by inventing a constant glass velocity c_g (now $c_{L\infty}$). We allowed for a weight increase of a fast relaxation process proportional to $(c_g^2-c_{L\alpha\infty}^2)$. Describing the fast spectrum by its low-frequency value τ_β allowed a formulation of the ''theoretical'' points $c_L(T)$ and $\Gamma_L(T)$ as a fit function of the global parameters. So we found, with a similar scenario to that described here, the missing widths of the Brillouin lines. The lack at that time was, that the relaxational spectrum was not properly normalized as it is now. But it introduced already the necessary philosophy, viz. a fast channel opening above T_g.

In the second previous study mentioned, the BS of $CaKNO_3$ was analyzed (backscattering geometry only). Li *et al.* [4] directly used the shape of the depolarized central line scattering to find the relaxational power of the fast β process. They claimed that this scattering is predominantly due to a DID scattering mechanism, and measures a density relaxation spectrum. In this way, they derived a $c_{L\alpha\infty}(T)$, and from this $f_{\mathrm{MCT}}(T)$, which shows a cusp shape as expected from MCT. They applied this procedure only for higher temperatures. There a single relaxation fit gives rise to an increase of $c_{L\alpha\infty}$, which is unphysical; we would find the same for *m*TCP if we would choose $\tilde{f}_L=1$.

The third study [19] derived for the supercooled As_2O_3 melt, the presence of a fast relaxational process ($\tau_\beta\approx 10$ ps) besides the slow α process, and relative weights 30:70, respectively, from Brillouin scattering and photon correlation spectroscopy. The authors suggested that the situation is similar in B_2O_3; both materials are among the strongest [1] glass-formers.

In the present work, we fit $\tilde{f}(T)$ directly. In this way we can start from an analytical ansatz for K_L and treat CL independently from LA or TA. Treating CL and LA or TA independently is suggested for *m*TCP by two facts: the CL is very strong, and presumably most of it is due to orientation fluctuations; and the CL width does not agree with Γ_α, as derived from LA or TA widths.

For density fluctuations the ratio of the moduli $c_0^2/c_{L\infty}^2$ governs the ratio of vibrational to relaxational (Mountain)

TABLE I. Parameters for *m*TCP. High and low frequency velocity parameters are from the fits. NMR relaxation time and T_g are from the literature.

Glass transition temperature :
$T_g = -68\,^\circ$ C$=205$ K
Velocity parameters (T in K, c in 10^3 m/s):
$c_{L\infty}(T) = 2.50 - 0.0040(T - T_g)$
$c_0(T) = 1.805 - 0.00326(T - T_g)$
$c_{T\infty}(T) = 1.15 - 0.0028(T - T_g)$
NMR relaxation time (T in K, τ in s) [11]:
$\ln[\tau_{\alpha,\mathrm{NMR}}(T)] = -33.08 + 2.272\times10^4/T - 7.851\times10^6/T^2 + 9.5255\times10^8/T^3$

intensity, Eq. (9). Turning now to the strong depolarized CL, considering it as given (a Mountain peak so to speak), one has to search for its vibrational excitations. The only candidate for a vibrational part is the boson peak [14]. But its intensity amounts for *m*TCP only to 10% of the central line intensity.

In [14] we also used the viscoelastic description for the boson peak of *m*TCP. This allows a partly quantitative description of the high-frequency wing below the boson peak maximum. Modulus parameters are taken from the present work; locally fitted $\tilde{f}$ values closely follow the values given in Fig. 5, and the Γ_β's are in the range from 50/150 GHZ increasing with T. The CL has all the time to be handled as an additional independent quantity.

Doing the reverse, namely, trying to fit Eq. (13) to the wide range HV spectra, we found values for $\tilde{f}_C$ in the range of a 0.97/0.99 instead of the values for $\tilde{f}$ plotted in Fig. 5. So we have to conclude that in *m*TCP the relaxational reorientation of the molecules is only governed by an α process, and this process is slower than the slow process for propagating LA waves.

B. The *f* parameters and the MCT scenario

The second item is the discussion of the weight factors. The value of $\tilde{f}(T)$ determines the relative strength of slow to fast relaxation, and thus the frequency dependent moduli; see Eqs. (3), (6), and (12). The value $\tilde{f}(T)$ changes from near 1 to near 0.4 between T_g and about $1.5T_g$; see Fig. 5. Its connection with the nonergodicity parameter f_{MCT} of the mode-coupling theory is given by Eq. (10), as a consequence of which f_{MCT} changes only from about 0.5 to 0.3. The reason is that the phonons are an essential part of the spectrum $\phi_N''(q,\omega)$.

Let us discuss the f factors by using their definition as an integral over the spectrum $\phi_N''(q,\omega)$, extending up to but not including the region of the phonon lines. Referring to the lower part of Fig. 6, and starting with the largest q and thus largest ω values, the phonon part of the integral over $\phi_N''(q,\omega)$ is $1 - f_{\mathrm{Total}}$ [Eq. (9)]. But the integral covers the full relaxation spectrum only if the phonon frequency is much larger than Γ_α and Γ_β (and therefore the apparent sound velocity is $c_{L\infty}$), so that the reduction of the integral by the phonon line cutoff (which is necessary for the second moment sum rule) is negligible.

If there is a large gap between Γ_α and Γ_β, as for temperatures near T_g, and we consider phonons with $\Gamma_\alpha < \omega_L < \Gamma_\beta$, the velocity is $c_{L\alpha\infty}$. But now the phonon intensity becomes $1 - f_{\mathrm{MCT}}$, which is larger than $1 - f_{\mathrm{Total}}$, i.e., larger than in the previous measurement.

A further increase takes place when the phonon frequency in the experiment is still lower, so that one has crossed the α-relaxation region and measures c_0. Now the intensity of the phonons reaches ~ 1; no intensity is left for the central part, because the vibrations generally cut off the part of the relaxational spectrum which is on their high-energy side (see Fig. 6) (entropy fluctuations are neglected). In Fig. 5 this is shown by the two lowest curves g_{Mount}, which are the integrals over $\phi_N''(q,\omega)$ up to half of the phonon frequency (displayed are the values for the ultrasonic and the Brillouin experiment, respectively). Slightly above T_g, they start with values near or equal to f_{MCT}, follow the latter closely up to their respective crossover temperature ($\omega\tau_\alpha \approx 1$), and then fall far below f_{MCT} for higher T. The phonon part $g_{\mathrm{Phon}}(T) = 1 - g_{\mathrm{Mount}}(T)$ is given as the increasing upper curve in Fig. 5.

These g curves were drawn here after having fitted the moduli and $\tilde{f}$ values using Eqs. (2) and (3). It would be useful to take them directly from experimental integrals over the phonon lines; however, one would have to introduce another intensity reference.

Analyses using only one relaxational process (α) as, were performed in Refs. [22–24], led sometimes to unreasonable (viz. nonmonotonic) temperature dependencies for $f_{\mathrm{MCT}}(T)$, (see Figs. 8 and 9 in Ref. [4], Figs. 14 and 16 in Ref. [22], or, for $c_o(T)$, Fig. 2 in Ref. [24]). Whether or not these problems are in fact due to a neglect of the fast relaxation process depends on whether in these cases the β process is much faster than the frequency scale of the measurement ($\Gamma_\beta \gg \omega_L$). Only if this condition is met is $c_{L\alpha\infty}$ a well measurable quantity, as is f_{MCT}; see Eq. (10). If, on the contrary, the condition $\Gamma_\beta \gg \omega_L$ is not fulfilled, as in the Brillouin experiment here, the β process has to be taken directly into account.

In the scenario discussed here, the temperature dependence of $\tilde{f}$ is the reason for the rapid decrease of the apparent sound velocities above T_g: when the temperature starts to rise above $T = 0$, the moduli soften slowly (below the $T \to 0$ values) as long as one is in the glass state, because the β-relaxation time and $\tilde{f}$ decreases slowly. (This action is seen very clearly in the BP region [25].) At T_g, the frozen in fluctuations first begin to melt, and $\tilde{f}(T)$ decreases much faster with increasing T, reducing the modulus correspond-

ingly for all frequencies below Γ_β.

This is the drop seen in $c_{L\alpha\infty}(T)$ for $T>T_g$. Around the temperature where $\omega\tau_\alpha\approx 1$, the apparent sound velocity c_L is brought down further from $c_{L\alpha\infty}$ to c_o when crossing through the α relaxation.

By taking into account both fast and slow relaxations and their relative weight explicitly, the determination of $\tilde{f}(T)$ from the Brillouin data becomes rather reliable (except when $\omega\tau_\alpha<1$, which happens in *m*TCP only above 50 °C, see Fig. 4).

Our results for $\tilde{f}$ show a change in slope around $T^*\approx 308K\approx 1.5T_g$. This value does not agree too well with the characteristic transition temperature (T_c of MCT) as found by an analysis of the softening of the BP for the case of *m*TCP, viz. $(1.2/1.3)T_g$; see Ref. [26].

The present data indicate, but are not sufficient to prove, the ''cusp'' shape of $f_{\mathrm{MCT}}(T)$, which MCT predicts. As just mentioned, anomalies were found in $c_\infty(T)$ or $c(T)$ in other works [19,24]; perhaps these data may indeed lead to clear cusps or breaks in $f_{\mathrm{MCT}}(T)$, if the analysis is performed in the way proposed here, i.e., taking two relaxation times into account.

The general difference between macroscopic (LA, TA) and microscopic (CL) motions, which was mentioned above in the discussion of τ_α, may also be a reason for the difference in temperature dependence between $\tilde{f}_L=\tilde{f}_T=\tilde{f}$ (T dependent, Fig. 5) and $\tilde{f}_C=1$ (T independent).

C. Bulk and shear excitations

As a third item we return to the viscoelastic description of LA and TA waves in terms of their complex moduli, $\tilde{M}_L(\omega)$ and $\tilde{M}_T(\omega)$ respectively. This is of interest in the context of MCT again, because MCT is conventionally applied to *density* fluctuations.

The two basic excitations of continuous media are bulk and shear deformations, with moduli $\tilde{B}(\omega)$ and $\tilde{G}(\omega)$ respectively, and the relations $\tilde{M}_L(\omega)=\tilde{B}(\omega)+\frac{4}{3}\tilde{G}(\omega)$ and $\tilde{M}_T(\omega)=\tilde{G}(\omega)$ are basic consequences of continuum mechanics. Since the present experiments furnish $\tilde{M}_L(\omega)=K_L(\omega)\rho/q^2$ and $\tilde{M}_T(\omega)=K_T(\omega)\rho/q^2$, it appears useful to go on to $\tilde{B}(\omega)$ and $\tilde{G}(\omega)$. Here we restrict the discussion to the high-frequency limit, where $B\approx\tilde{B}(\omega)\gg|\mathrm{Im}\{\tilde{B}(\omega)\}|$, $G\approx\tilde{G}(\omega)\gg|\mathrm{Im}\{\tilde{G}(\omega)\}|$ and

$$c_{L\infty}^2=\left(B+\frac{4}{3}G\right)\Big/\rho, \tag{14}$$

$$c_{T\infty}^2=G/\rho. \tag{15}$$

This limit is fulfilled when ''the high-frequency values'' for c_L and c_T are used. [One might be tempted to use for B the value of $c_o^2\rho$, extrapolated simply linearly from high to low temperature assuming that c_o was the c_L value when $G\approx 0$. Inspection of Fig. 2 for $T\approx T_g$ shows, however, that Eq. (14) is not fulfilled there. From the figure we find $c_L^2=6.2\times 10^6$ m^2/s^2, while the right-hand side of Eq. (14) is 4.8×10^6 m^2/s^2, an inconsistency far above the error bar. The error occurs because $c_0(T)$ changes just above T_g; see below.]

To solve for B and G, we remember that the ''sound velocities with negligible relaxation,'' are $c_{L\infty}$ and $c_{T\infty}$, respectively, as introduced above; they lie slightly above the values observed at T_g in Brillouin and ultrasonic experiments; see Fig. 2. Thus we can evaluate B or the related sound velocity $c_{B\infty}=(B/\rho)^{1/2}$ from Eqs. (14) and (15). The result, $c_{B\infty}=2.1\times 10^3$ m/s at T_g, appears in Fig. 2 as the open square. Bulk modulus values were evaluated from ultrasonic data for several materials (see, e.g., Refs. [27,28]), but to our knowledge from Brillouin data only for $BiCl_3$-KCl [29].

It was already mentioned in Sec. V B that $\tilde{f}(T)$ shows a break at $T^*=1.5T_g$, not far from the temperature where a characteristic change of dynamics has been detected [26] by an analysis of the BP. We assume here that these are two different aspects of the same underlying phenomenon, which in MCT is the critical temperature T_c.

According to the usual interpretation of MCT the additional nonergodic processes which freeze in below T_C should be density fluctuations. Let us regard the fluctuations at small and intermediate q. Density fluctuations are of the order $\langle\delta\rho^2\rangle\approx k_BT/c_B^2$. If one were to draw into Fig. 2 the curve for the temperature dependence $c_B(T)$ at, say, $\omega\approx 10^{11}$ rad/s, it would drop from the open square, $c_{B\infty}$, toward $c_o(T)$ in the same way in which $c_L(T)$ drops from $c_{L\infty}$ and approaches $c_o(T)$. [At present we see no reason to doubt that the $\tilde{f}$ factor for bulk excitations obeys $\tilde{f}_B(T)\approx\tilde{f}(T)$, and that the same time constants τ_α, τ_β apply.] The cusp height for these small q density fluctuations is thus of the order of the relative change of B between $c_{B\infty}^2$ and c_0^2, which is 10/15%. Such a relatively small change of density fluctuations does not *a priori* speak against density fluctuations as the relevant variable in MCT.

However, the relative change of shear wave fluctuations $[k_BT/c_T(T)^2]$ around the same temperature is much larger: 100%. Therefore, in our view the question should be taken up again, about which of the two may be the driving mechanism for the liquid-glass transformation. In terms of MCT, the question is the following: What is the quantity for which the dynamic nonlinear feedback mechanism becomes active (and which then ''slaves'' the other one)? It appears that the low-frequency excitations, which are predominantly shear or librations, would qualify easily for any nonlinear mechanism because they do have large amplitudes ($k_BT/\hbar\omega\gg 1$). Dense packing will also supply sufficient feedback for shear motions. The argument that, in principle, shear fluctuations cannot persist forever on theoretical grounds may not be as stringent when real glass-formers are considered.

ACKNOWLEDGMENTS

The authors are indebted to A. Spiroski and A. Kisliuk for important experimental contributions. D.Q. appreciates helpful discussions with V.A. Solovyev which were made possible by INTAS. This work was supported by DFG through Grant No. Sfb 337. We are very grateful to F. W. Deeg and Karen Diercksen for their permission to include their ISTS data into the present analysis.

[1] J. Wong and C. A. Angell, *Glass* (Dekker, New York, 1976).
[2] U. Bengtzelius, W. Goetze, and A. Sjoelander, J. Phys. C **17**, 5915 (1984); W. Goetze and L. Sjoegren, Rep. Prog. Phys. **55**, 241 (1992).
[3] S. Loheider, G. Vögler, I. Petscherizin, M. Soltwisch, and D. Quitmann, J. Chem. Phys. **93**, 5436 (1990).
[4] G. Li, W. M. Du, J. Hernandez, and H. Z. Cummins, Phys. Rev. E **48**, 1192 (1993).
[5] A. R. Duggal and K. A. Nelson, J. Chem. Phys. **94**, 7677 (1991).
[6] F.W. Deeg and K. Diercksen (unpublished).
[7] E. Leutheuser, Phys. Rev. A **29**, 2765 (1984); T. Geszti, J. Phys. (Paris) Colloq. **43**, C9-435 (1982).
[8] S. P. Das and G. F. Mazenko, Phys. Rev. A **34**, 2265 (1986); J. J. Ullo and S. Yip, Phys. Rev. Lett. **54**, 1509 (1985).
[9] J. Bosse and J. S. Thakur, Phys. Rev. Lett. **59**, 998 (1987); J. S. Thakur and J. Bosse, Phys. Rev. A **43**, 4378 (1991); **43**, 4388 (1991).
[10] H. Z. Cummins, G. Li, W. Du, R. M. Pick, and C. Dreyfus, Phys. Rev. E **53**, 896 (1996).
[11] E. Roessler, A. P. Sokolov, P. Eiermann, and U. Warschewske, Physica A **201**, 237 (1993); E. Roessler and P. Eiermann, J. Chem. Phys. **100**, 5237 (1994).
[12] E. Riande, H. Markovitz, D. J. Plazek, and N. Raghupathi, J. Polym. Sci. **50**, 405 (1975).
[13] V. Mazzacurati, P. Benassi and G. Ruocco, J. Phys. E **21**, 798 (1988).
[14] M. Soltwisch, G. Monaco, G. Ruocco, and D. Quitmann, Philos. Mag. (to be published).
[15] M. Soltwisch, A. Spiroski, A. Kisliuk, A. P. Sokolov, E. Roessler, and D. Quitmann, Philos. Mag. B **71**, 683 (1995).
[16] G. Arachovitis, B. Balschun, M. Soltwisch, and D. Quitmann, J. Chem. Phys. **103**, 9574 (1995).
[17] B. J. Berne and R. Pecora, *Dynamic Light Scattering* (Wiley, New York, 1976).
[18] D. Quitmann, M. Soltwisch, and G. Ruocco, J. Non-Cryst. Solids **203**, 12 (1996).
[19] S. N. Yannopoulos, G. N. Papatheodorou, and G. Fytas, Phys. Rev. E **53**, R1328 (1996).
[20] See Fig. 5 of A. Kisliuk, S. Loheider, A. P. Sokolov, M. Soltwisch, D. Quitmann, E. Shasha and A. Voronel, Phys. Rev. B **52**, 13 083 (1995).
[21] G. Floudas, J. S. Higgins, and G. Fytas, J. Chem. Phys. **96**, 7672 (1992).
[22] W. M. Du, G. Li, H. Z. Cummins, M. Fuchs, J. Toulouseaud, and L. A. Knauss, Phys. Rev. E **49**, 2192 (1994).
[23] C. Dreyfus, M. J. Lebon, H. Z. Cummins, J. Toulouse, B. Bonello, and R. Pick, Phys. Rev. Lett. **69**, 3666 (1992).
[24] M. Elmroth, L. Boerjesson, and L. M. Torell, Phys. Rev. Lett. **68**, 79 (1992).
[25] M. Krueger, M. Soltwisch, I. Petscherizin, and D. Quitmann, J. Chem. Phys. **96**, 7352 (1992).
[26] A. P. Sokolov, A. Kisliuk, D. Quitmann, A. Kudlik, and E. Roessler, J. Non-Cryst. Solids **172-174**, 138 (1994).
[27] K.F. Herzfeld and T.A. Litovitz, *Absorption and Dispersion of Ultrasonic Waves* (Academic, New York, 1959).
[28] R. S. Marvin and J. E. McKumey in *Physical Acoustics*, edited by W. P. Mason (Academic, New York, 1965), Vol. IIB, p. 165 (1965).
[29] L. M. Torell, J. Non-Cryst. Solids **56**, 93 (1983).